agronomy

MDPI

Article

FTIR Screening to Elucidate Compositional Differences in Maize Recombinant Inbred Lines with Contrasting Saccharification Efficiency Yields

Ana López-Malvar [1,2,*], Rogelio Santiago [1], Rosa Ana Malvar [2], Daniel Martín [3], Inês Pereira dos Santos [3], Luís A. E. Batista de Carvalho [3], Laura Faas [4], Leonardo D. Gómez [4] and Ricardo M. F. da Costa [3,5]

1 Facultad de Biología, Departamento de Biología Vegetal y Ciencias del Suelo, Universidad de Vigo, As Lagoas Marcosende, 36310 Vigo, Spain; rsantiago@uvigo.es
2 Misión Biológica de Galicia (CSIC), Pazo de Salcedo, Carballeira 8, 36143 Pontevedra, Spain; rmalvar@mbg.csic.es
3 Molecular Physical-Chemistry R&D Unit, Department of Chemistry, University of Coimbra, Rua Larga, 3004-535 Coimbra, Portugal; dmfernandez@uc.pt (D.M.); ips@uc.pt (I.P.d.S.); labc@ci.uc.pt (L.A.E.B.d.C.); rmfdcosta@uc.pt (R.M.F.d.C.)
4 Centre for Novel Agricultural Products, Department of Biology, CNAP, University of York, York YO10 5DD, UK; laura.faas@york.ac.uk (L.F.); leonardo.gomez@york.ac.uk (L.D.G.)
5 Centre for Functional Ecology, Department of Life Sciences, University of Coimbra, Calçada Martim de Freitas, 3000-456 Coimbra, Portugal
* Correspondence: alopezmalvar@mbg.csic.es

check for updates

Citation: López-Malvar, A.; Santiago, R.; Malvar, R.A.; Martín, D.; Pereira dos Santos, I.; Batista de Carvalho, L.A.E.; Faas, L.; Gómez, L.D.; da Costa, R.M.F. FTIR Screening to Elucidate Compositional Differences in Maize Recombinant Inbred Lines with Contrasting Saccharification Efficiency Yields. *Agronomy* **2021**, *11*, 1130. https://doi.org/10.3390/agronomy11061130

Academic Editor: Lorenzo Cotrozzi

Received: 3 May 2021
Accepted: 31 May 2021
Published: 2 June 2021

Abstract: With a high potential to generate biomass, maize stover arises as an outstanding feedstock for biofuel production. Maize stover presents the added advantage of being a multiple exploitation of the crop as a source of food, feed, and energy. In this study, contrasting groups of recombinant inbred lines (RILs) from a maize multiparent advanced generation intercross (MAGIC) population that showed variability for saccharification efficiency were screened by FTIR-ATR spectroscopy to explore compositional differences between high and low saccharification yielders. High and low saccharification efficiency groups differed in cell wall compositional features: high saccharification RILs displayed higher proportions of S subunits, aromatic compounds, and hemicellulose as opposed to low saccharification efficiency groups in which FTIR predicted higher proportions of lignin, more precisely lignin being richer in subunits G, and greater proportions of crystalline cellulose and acetyl methyl esters. The application of FTIR-ATR spectroscopy in this material allowed us to obtain a rapid and broad vision of cell wall compositional features in contrasting groups of saccharification efficiency. These results helped us to deepen our knowledge into the relationship between cell wall composition and biorefining potential; they also allowed us to establish new targets for future research regarding lignocellulosic bioconversion.

Keywords: FTIR-ATR; saccharification efficiency; cell wall; MAGIC

1. Introduction

Besides its uses as food and feed, maize stover after ear removal can have biorefinery applications. Cellulosic ethanol derived from fast growing C4 crops has become one of the preferred alternatives to fossil fuels due to their high biomass yields, broad geographic adaptation, carbon sequestration, and nutrient utilization [1,2]. Maize has a high biomass yield potential (5.2 tons of dry matter/ha; dry biomass yield) and has been proposed as an outstanding model for biofuel production [3,4].

Lignocellulosic feedstock, such as maize stover, is highly abundant and readily available as substrates for second-generation biofuel production [1,5]. It is typically composed of 39.4% cellulose, 33.1% hemicelluloses, and 14.9% lignin [6]. Lignin concentration and composition present variations among taxa and tissue types [7]. In mature stalk, G and S

lignin units are prevalent compared to H units with average ratios that are nearly equal to 35% and 4%, respectively [8].

The conversion of lignocellulosic biomass to ethanol is a three-step process, namely (i) a pretreatment stage, followed by (ii) a hydrolytic degradation of carbohydrates to the constituent sugar monomers (saccharification), and (iii) a final fermentation of the free sugars to ethanol [9]. The main obstacle for the biomass fermentation process is cell wall recalcitrance, defined as cell wall resistance to degradation by microbial cellulolytic complex. Recalcitrance increases the energy requirements, the cost, and complexity of bio refinery operations and reduce the recovery of biomass carbon into desired products [10]. Therefore, the reduction of cell wall recalcitrance by overcoming chemical and structural properties of the cell wall is expected to improve saccharification efficiency and increase the sugars that could be fermented [11].

The saccharification process is dependent on the composition and architecture of the cell wall. One of the key traits for the processing of plant biomass to produce biofuels and biomaterials is cell wall quality [12,13]. Efforts to reduce the inherent recalcitrance of bioenergy feedstock have focused on understanding how variations in lignin content, composition, and structure can alter the bioconversion process. Lignin reduces the efficacy of enzymatic saccharification processes by adsorbing and nonproductively binding to hydrolytic enzymes [14,15] and by physically shielding cellulose microfibrils from enzymatic attack [12]. The variations in lignin monomeric composition (such as the way lignin monomers are linked or the increase in S-lignin proportions) have proven useful for enhancing extraction efficiency. A key determinant of cell wall architecture are crosslinks between polysaccharides and lignin via hydroxycinnamates [12]. These bonds restrict the accessibility of exogenous enzymes to the cell wall polysaccharides, hindering biomass hydrolysis [6,13]. Finally, the degree of polymerization of the cellulose and its crystallinity index have also been associated to reductions in biomass recalcitrance [15–17].

López-Malvar et al. [18] evaluated a subset of recombinant inbred lines (RILs) derived from a multiparent advanced generation intercross (MAGIC) population, and they found variability for saccharification efficiency in samples of maize stover after alkaline pretreatment. From that RIL subset, we selected the lines showing the highest and lowest saccharification efficiency, and in the current study we screen them by Fourier-transform infrared spectroscopy in attenuated total reflectance mode (FTIR-ATR) which, in contrast to analytical/biochemical methods, is a rapid, noninvasive and powerful high-throughput tool to study the cell wall. This technique has been extensively used for the study of the cell wall components, crosslinking, and carbohydrate constituents and their organization [19,20].

The aim of this study is to take advantage of this spectroscopy technique applied to contrasting saccharification efficiency groups in order to elucidate differences in the cell wall composition and architecture of high and low sugar-yielding RILs. In addition, as far as we know, this is first time that FTIR-Principal Component Analysis is used on maize RILs to correlate cell wall traits with saccharification. It is expected that the results obtained in this research will show the relationship between the composition of the wall and the cellulose bioconversion process in stover samples from highly variable RILs, which could reveal key aspects to optimize the conversion of not only lignocellulosic biomass biorefinery but also other promising bioproducts such as biogas via fermentation with anaerobic bacteria or nonbiofuel-related products derived from fermentation of lignocellulose derived sugars.

2. Material and Methods

A subset of 408 RILs and the eight founders of a MAGIC population developed by the Maize Genetics and Breeding group at Misión Biológica de Galicia-CSIC [21,22] were evaluated in single augmented design with 10 blocks in Pontevedra for two years (2016, 2017). Saccharification efficiency was considered as the amount of released sugars (nmol mg^{-1} $material^{-1}$ h^{-1}) after alkaline pretreatment: 0.5 M NaOH at 90 °C for 30 min, washed four times with 500 µL sodium acetate buffer, and subjected to enzymatic digestion

(Celluclast CTec2, 7FPU/g) at 50 °C for 8 h [23]. For detailed material and methods determination, see López-Malvar et al. [18]

2.1. Fourier-Transform Infrared Spectroscopy

Attenuated total reflectance Fourier transform mid-infrared (FTIR-ATR) spectroscopy was performed on all samples included in this study, as reported elsewhere [20,24]. Duplicate spectra were collected in the range 4000–400 cm^{-1} using a Bruker Optics Vertex 70 FTIR spectrometer purged by CO_2-free dry air and equipped with a Brucker Platinum ATR single reflection diamond accessory. A Ge on KBr substrate beamsplitter and a liquid nitrogen-cooled wide-band mercury cadmium telluride (MCT) detector were used. Spectra were averaged over 32 scans at a resolution of 4 cm^{-1}, and the 3-term Blackman–Harris apodization function was applied. The Bruker Opus 8.1 software was also used for (i) removing eventual H_2O and CO_2 contributions and (ii) spectral smoothing using the Savitzky–Golay algorithm. Absorbance spectra were further preprocessed using in-house built functions in MATLAB (v. R2014b; MathWorks, Natick, MA, USA). Full spectra, or fingerprint region spectra (1800–800 cm^{-1}), were averaged (per replicate), vector normalized to unit length, and the baseline was removed according to the automatic weighted least squares algorithm (polynomial order = 2) prior to statistical analysis, using the Eigenvector PLS Toolbox (v. 7.9; Eigenvector Research, Wenatchee, WA, USA). For the t-tests on spectral data to unveil the underlying chemometric relationships between FTIR-ATR spectra, an R-based data analysis platform was used [Chong 2018-https://doi.org/10.1093/nar/gky310 (accessed on 1 August 2020)].

2.2. Statistical Analysis

An analyses of variance was done for saccharification efficiency according to the SAS mixed-model procedure (PROC MIXED) of the SAS program, version 9.4 (SAS Institute 2015). Inbred lines were considered as the fixed effects, while years, replication within years, and lines × year were considered random effects. The comparison of means among inbred lines was carried out using Fisher's protected least significant difference (LSD). In order to classify the RILs into high- and low-saccharification groups, data from each year were considered separately since we observed the RIL x year interaction. From each year we selected a total of 60 RILs according to its saccharification efficiency (30 high yielders, 30 low yielders). High and low groups differed significantly in their saccharification efficiency (LSD < 0.01).

3. Results and Discussion

A subset of 408 RILs from a maize MAGIC population were evaluated for saccharification efficiency and analyzed by FTIR-ATR spectroscopy in field experiments over two years.

RILs differed significantly for saccharification efficiency (Supplementary Table S1). A total of 778 samples of maize ground biomass were analyzed in duplicate by FTIR-ATR spectroscopy, for a total of 1556 data points. A preliminary principal component analysis (PCA) model was calculated, including all the data. No natural data clusters were detected, suggesting that the samples were not significantly distinct from each other.

We observed a large influence of the year for saccharification efficiency, but we did not observe a yearxgenotype interaction, indicating that even though saccharification efficiency value ranges are different for each year, RILs that in one year present high saccharification efficiency would also present high values in the other year (data not shown).

Using the information from the best linear unbiased estimator (BLUEs) from each year, the 30 lowest and the 30 highest lines according to the saccharification yields were selected to form two extreme groups (Table 1). A t-test ($p \leq 0.001$) was performed for each variable (wavenumber) to compare between high- and low-saccharification groups. For the 2016 assay, 208 variables were significantly different, whereas for 2017, 121 variables were significantly different. Two PCA models (2016 and 2017) were calculated based

on these highly significantly different variables. In both cases, separation between high- and low-saccharification groups occurred along PC1 (Figure 1). Subsequently, based on PC1 loadings, tentative compositional attributions were made (Table 2) in order for us to understand the underlying relationships between the groups of spectra.

Table 1. Saccharification efficiency data, means, and range for two years (2016, 2017) in selected RILs from a MAGIC population classified in high and low saccharification yielders.

2016		2017	
RILs	**Saccharification (nmol mg^{-1} material^{-1} h^{-1})**	**RILs**	**Saccharification (nmol mg^{-1} material^{-1} h^{-1})**
	Low		
EPS21LR-415	70.354	EPS21LR-267	138.409
EPS21LR-494	73.340	EPS21LR-280	140.569
EPS21LR-629	77.574	EPS21LR-560	142.657
EPS21LR-711	78.112	EPS21LR-347	142.719
EPS21LR-289	78.183	EPS21LR-283	142.979
EPS21LR-748	78.336	EPS21LR-409	143.652
EPS21LR-472	79.001	EPS21LR-597	143.789
EPS21LR-643	79.213	EPS21LR-703	143.864
EPS21LR-414	79.443	EPS21LR-260	144.628
EPS21LR-526	79.588	EPS21LR-698	144.732
EPS21LR-316	80.571	EPS21LR-522	148.238
EPS21LR-353	80.747	EPS21LR-670	149.194
EPS21LR-547	81.101	EPS21LR-614	149.238
EPS21LR-317	81.409	EPS21LR-348	150.578
EPS21LR-698	81.641	EPS21LR-398	150.623
EPS21LR-753	82.205	EPS21LR-284	151.153
EPS21LR-675	82.983	EPS21LR-578	152.176
EPS21LR-416	82.984	EPS21LR-619	152.182
EPS21LR-524	83.346	EPS21LR-514	152.870
EPS21LR-285	83.747	EPS21LR-617	152.978
EPS21LR-750	83.753	EPS21LR-427	153.046
EPS21LR-522	83.909	EPS21LR-414	153.132
EPS21LR-426	83.936	EPS21LR-462	153.548
EPS21LR-284	83.998	EPS21LR-669	153.581
EPS21LR-759	84.292	EPS21LR-253	154.624
EPS21LR-251	84.670	EPS21LR-740	155.013
EPS21LR-378	84.768	EPS21LR-361	155.073
EPS21LR-677	85.155	EPS21LR-682	155.156
EPS21LR-257	85.341	EPS21LR-411	155.316
EPS21LR-478	85.468	EPS21LR-276	155.693
Means	81.306	Means	149.380
Range	70.354–85.468	Range	138.409–155.693

Table 1. *Cont.*

2016		2017	
RILs	**Saccharification (nmol mg^{-1} material^{-1} h^{-1})**	**RILs**	**Saccharification (nmol mg^{-1} material^{-1} h^{-1})**
	High		
EPS21LR-749	114.589	EPS21LR-539	196.892
EPS21LR-623	114.671	EPS21LR-304	196.911
EPS21LR-663	114.899	EPS21LR-325	196.961
EPS21LR-395	115.104	EPS21LR-483	197.079
EPS21LR-259	115.128	EPS21LR-753	197.152
EPS21LR-261	115.189	EPS21LR-646	197.893
EPS21LR-243	115.207	EPS21LR-598	198.361
EPS21LR-489	115.817	EPS21LR-451	199.220
EPS21LR-337	116.051	EPS21LR-396	200.177
EPS21LR-473	116.829	EPS21LR-442	200.615
EPS21LR-657	117.058	EPS21LR-655	201.290
EPS21LR-709	117.321	EPS21LR-381	201.830
EPS21LR-325	117.476	EPS21LR-515	202.263
EPS21LR-653	117.506	EPS21LR-672	203.171
EPS21LR-720	117.547	EPS21LR-482	203.753
EPS21LR-503	117.935	EPS21LR-259	203.789
EPS21LR-405	118.170	EPS21LR-487	204.326
EPS21LR-695	118.372	EPS21LR-412	204.728
EPS21LR-512	118.901	EPS21LR-343	204.963
EPS21LR-726	119.333	EPS21LR-517	205.161
EPS21LR-560	119.530	EPS21LR-741	205.377
EPS21LR-514	120.591	EPS21LR-547	205.750
EPS21LR-741	120.596	EPS21LR-395	205.809
EPS21LR-733	120.959	EPS21LR-508	206.084
EPS21LR-668	121.101	EPS21LR-248	208.187
EPS21LR-364	121.287	EPS21LR-723	209.809
EPS21LR-246	121.350	EPS21LR-694	211.761
EPS21LR-584	123.927	EPS21LR-594	212.177
EPS21LR-511	125.722	EPS21LR-679	218.327
EPS21LR-743	127.652	EPS21LR-502	218.694
Means	118.527	Means	203.950
Range	114.589–127-652	Range	198.892–218.694

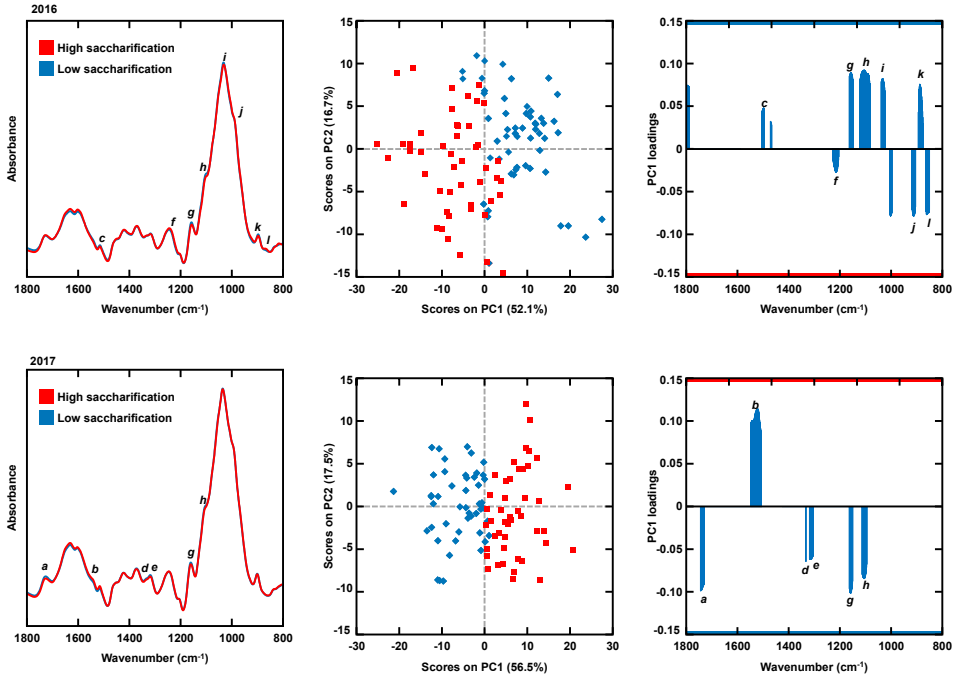

Figure 1. Mean FTIR-ATR spectra of maize lignocellulosic biomass from high and low saccharification yield groups, harvested in 2016 and 2017, in the range 1800–800 cm^{-1}. Score plot of the PCA model calculated based on highly significantly different variables ($p \leq 0.001$), as calculated by t-tests (208 variables for 2016 and 121 variables for 2017). The PC loadings plots indicate spectral regions (*a*–*l*) that are positively or negatively correlated to PC1, along which group separation occurred. Table 2 shows the wavenumbers corresponding to each region.

In the 2016 model, the high-saccharification group was clustered on the negative portion of PC1, which is negatively correlated with spectral bands ascribed to the molecular features associated to syringyl (S-lignin) units (*f*), aromatic compounds (*j*), and to hemicelluloses (*l*) (Table 2, Figure 1) [24–29]. By contrast, PC1 is positively correlated with spectral regions ascribed to lignin structural features, namely to guaiacyl (G-lignin) units (*c*, *h*, and *i*), and to cellulose structural features, e.g., to crystalline cellulose (*g* and *k*) (Table 2, Figure 1) [26,28,30–36]. Given that the low-saccharification group is mostly clustered on the positive side of PC1, samples classified as low yielders were predicted to have higher proportions of these compositional and structural cell wall traits.

In the 2017 model, the high-saccharification group is clustered on positive regions of PC1, which is negatively correlated to the following structural features: acetyl and methyl esters (*a*), lignin (*h*), and cellulose structural features (*d* and *e*), such as its degree of crystallinity (*g*) (Table 2, Figure 1) [30–45].

Table 2. Assignment of relevant FTIR-ATR absorption bands characteristic of maize cell wall biomass.

PC1 Loading Spectral Region	Wavenumber (cm^{-1})	Reference	Assignment	Biomass Constituent
a	1740 1735 1734	[37,40,43,44]	C=O stretching	Acetyl and methyl esters
b	1550	[29,30,37]	Amide II (N-H deformation and stretching contribution from C-N stretching)	Proteins

Table 2. *Cont.*

PC1 Loading Spectral Region	Wavenumber (cm^{-1})	Reference	Assignment	Biomass Constituent
c	1504 1500	[26,28]	Aromatic skeletal vibrations in guaiacyl rings	Lignin
d	1336	[38,41]	C-H in plane deformation	Cellulose
e	1328 1311 1318 1311	[38,39,43–46]	OH in-plane bending CH_2 wagging CH in plane scissoring	Cellulose
f	1224 1219 1220	[27,28]	C–O stretch in syringyl rings	Lignin
g	1160 1161 1163 1157	[30–35]	C–O–C asymmetric stretching	Crystalline cellulose; associated to modifications cellulose-I > cellulose-II; linked to celluloses crystallinity features
h	1116	[31,36]	Aromatic C–H deformation	Lignin
i	1035 1041 1040	[24,29,47]	Aromatic C–H in plane deformation, G > S; plus C–O deformation in primary alcohols; plus C=O stretch (unconjugated)	Lignin
j	915–925	[24,29]	C-H out-of-plane; aromatic compounds	Aromatic compounds
k	898	[35]	C–O–C stretching	Cellulose
l	872 875	[25]	Glycosidic linkage in hemicelluloses	Hemicellulose

Biomass hydrolysis is a key factor in lignocellulosic deconstruction during biofuel production. Among other cell wall components such as ester linked hydroxycinnamates or arabinose/xylose ratio, lignin has been pointed out as one of the most important polymer in the determination of biomass recalcitrance, not only because it makes the biomass resistant to digestion, but also because lignin fractions adsorb enzymes, reducing their access to the polysaccharides [47–49]. Reductions in lignin content are positively correlated with increases of cell wall hydrolysis efficiency [50,51]. This is supported by the results obtained in this study, as higher saccharification yields in 2017 are related with FTIR predictions of decreasing concentrations of lignin. Besides total lignin content, its composition and the manner in which it binds holocellulose within the cell wall matrix is often seen as a feature of cell wall recalcitrance to enzymatic deconstruction [47]. Modifications in the phenylpropanoid pathway, through enzymes directly changing lignin content and monolignol composition, were associated with increases in saccharification efficiency in several crops [52]. For example, transgenic switchgrass lines with reduced cinnamyl alcohol dehydrogenase (CAD) levels and consequently reduced lignin content and altered lignin composition showed improved sugar release [53]. Similarly, Fornalé et al. [54] studied the effect of CAD downregulation on lignin S/G ratio, among other cell wall components, through a transgenic approach in maize. They observed a decrease in the syringyl-to-guaiacyl (S/G) ratio by both a reduction in the syringyl (S) subunits and an increase of the guaiacyl (G) and p-hydroxyphenyl (H) subunits. Moreover, they observed that transgenic plants produced 8% more cellulosic bioethanol than the wild type. The results obtained in the present study support the idea that lignin monomeric composition influences the saccharification efficiency of the feedstock. High saccharification yields in this MAGIC

population correlate with lignin subunits, i.e., lower proportions of G subunits in contrast to higher proportions of S subunits, which are known to promote saccharification efficiency. S units can only form β-O-4- (β-aryl ether) inter-unit linkages, which are easily cleaved onto. By contrast, G units have the availability of the C5 position for coupling. Lignin composed mainly of G units contain more resistant (β-5, 5-5, and 4-O-5) linkages than lignins incorporating S units [55,56].

However, variation in cell wall recalcitrance is not only due to lignin content and composition. In concordance with the results obtained, cell wall aromatic compounds, such as ferulic acid, could be positively correlated to saccharification in grass species [57]. To support this, FTIR predicted that RILs classified in the low saccharification efficiency group would present lower proportions of aromatic compounds.

On the other hand, lignocellulosic polysaccharides, mainly cellulose (40%), serve as the main substrate for the fermentation of cell wall sugars in ethanol. In this way, cell walls richer in cellulose have more sugars to potentially be fermented. The low-saccharification groups in 2017 were predicted to present lower proportions of cellulose structural features, which are detrimental for biomass deconstruction. The results obtained in 2016 show that low-saccharification groups presented higher cellulose crystallinity, indicating that crystallinity limit enzymatic degradability. Cellulose is composed of linear chains of D-glucopyranose residues linked by β-(1-4) glucosidic bonds that result in the formation of glucose dimers between adjacent chains that form a flat structure called cellobiose that is repeated. The structure of the cellulose chains allows for the formation of intermolecular hydrogen bridges. This results in a stable crystalline structure that provides cellulose mechanical strength and stability, contrasting with amorphous less organized regions [58]. The crystalline structure limits the penetration of water molecules and is highly resistant to chemical and biological hydrolysis to form fermentable sugars [10,57,59,60], thus decreasing saccharification efficiency and hydrolysis yield potential.

The interaction between cellulose and other cell wall features, such as the pattern of xylan acetylation, also influences saccharification since a uniform pattern of xylan substitution is crucial within plant cells interactions with cellulose [61]. In grass cell walls, most of the acetylation occurs in arabinoxylans, which modifies the interaction with cellulose and lignin [62]. The role of acetylation in biomass recalcitrance was demonstrated in other Poales species, such as in *Miscanthus* spp. [57]. In this study, we suggest that acetate could cause steric hindrance of hydrolytic enzymes, thus inhibiting both saccharification and fermentation. Pawar et al. [63] found that aspen plants with reduced xylan acetylation showed 25% higher glucose saccharification yield compared with wild types. They proposed that de-acetylating xylan increases susceptibility to hydrolytic enzymes during saccharification as well as promoting changes in the cell wall architecture that increase the extractability of lignin and xylan.

4. Conclusions

This study is one of the first research that used FTIR-PCA on maize RILs to correlate cell wall traits with saccharification. High- and low-saccharification groups differed in its cell wall spectral features, and FTIR spectroscopy in this material revealed proper cell wall compositional features for saccharification efficiency. The results presented here help us to understand the relationship between maize cell wall composition and its potential for biofuel production. This can allow for establishing new targets for future research and breeding targets to tailor biorefinery feedstock, for which this maize MAGIC population is a useful genetic tool that presents great advantages, such as high genetic diversity and rapid linkage disequilibrium decay.

Supplementary Materials: The following are available online at https://www.mdpi.com/article/10.3390/agronomy11061130/s1, Table S1. Average, range values and BLUEs for saccharification efficiency in RILs of the MAGIC population.

Author Contributions: A.L.-M., R.M.F.d.C., R.A.M., and R.S. conceived and design the study. R.A.M., R.S., and A.L.-M. participated in its design and carried out the field trial and participated in sample collection; A.L.-M. wrote the manuscript; L.F. and L.D.G. performed saccharification efficiency analysis and contributed to the discussion of the manuscript; A.L.-M. and R.A.M. participated in saccharification efficiency data analysis; R.M.F.d.C. performed FTIR-ATR and statistical analysis; D.M. participated in spectral interpretation of FTIR-ATR; I.P.d.S. participated in statistical analysis of FTIR-ATR; L.A.E.B.d.C. is responsible for the FTIR equipment, and contributed significantly to the discussion of the manuscript. All authors have read and agreed to the published version of the manuscript.

Funding: This research has been developed in the frame of the Agri-Food Research and Transfer Centre of the Water Campus (CITACA) at the University of Vigo (Spain), which is economically supported by the Galician Government and in the Misión Biológica de Galicia (CSIC). It was funded by the "Plan Estatal de Ciencia y Tecnología de España" (projects RTI2018–096776-B-C21, and RTI2018–096776-B-C22 cofinanced with European Union funds under the FEDER program). The funding body played no role in study design, data analysis, and manuscript preparation. Further support for the FTIR-ATR analyses came from the Project "RENATURE–Valorisation of the Natural Endogenous Resources of the Centro Region" (CENTRO-01-0145-FEDER-000007) and the Portuguese Foundation for Science and Technology (UIDB00070/2020).

Institutional Review Board Statement: Not applicable.

Informed Consent Statement: Not applicable.

Data Availability Statement: The data sets used and/or analyzed during the current study will be available upon request to the corresponding author. Vegetal materials are distributed to the scientific community by Maize Genetics and Breeding group of MBG-CSIC upon request (http://www.mbg.csic.es/en/plant-genetics-and-breeding-department/maize-genetics-and-breeding/rmalvar@mbg.csic.es).

Conflicts of Interest: Authors declare that they have no conflict of interest.

References

1. Vermerris, W.; Saballos, A.; Ejeta, G.; Mosier, N.S.; Ladisch, M.R.; Carpita, N.C. Molecular breeding to enhance ethanol production from corn and sorghum stover. *Crop Sci.* **2007**, *47*, S142. [CrossRef]
2. Van der Weijde, T.; Alvim Kamei, C.L.; Torres, A.F.; Vermerris, W.; Dolstra, O.; Visser, R.G.F.; Trindade, L.M. The potential of C4 grasses for cellulosic biofuel production. *Front. Plant Sci.* **2013**, *4*, 1–18. [CrossRef]
3. Vermerris, W. Cell wall Biosynthetic Genes of Maize and their Potential for Bioenergy Production. In *Handbook of Maize*; Springer: New York, NY, USA, 2009.
4. Courtial, A.; Soler, M.; Chateigner-Boutin, A.-L.; Reymond, M.; Mechin, V.; Wang, H.; Grima-Pettenati, J.; Barriere, Y. Breeding grasses for capacity to biofuel production or silage feeding value: An updated list of genes involved in maize secondary cell wall biosynthesis and assembly. *Maydica* **2013**, *58*, 67–102.
5. Dhugga, K.S. Maize biomass yield and composition for biofuels. *Crop Sci.* **2007**, *47*, 2211–2227. [CrossRef]
6. Pauly, M.; Keegstra, K. Cell-wall carbohydrates and their modification as a resource for biofuels. *Plant J.* **2008**, *54*, 559–568. [CrossRef] [PubMed]
7. Vanholme, R.; Cesarino, I.; Rataj, K.; Xiao, Y.; Sundin, L.; Goeminne, G.; Kim, H.; Cross, J.; Morreel, K.; Araujo, P.; et al. Genotypic variation in phenolic components of cell-walls in relation to the digestibility of maize stalks. *Plant Physiol.* **2010**, *11*, 1–18. [CrossRef]
8. Lapierre, C. Application of New Methods for the Investigation of Lignin Structure. In *Forage Cell Wall Structure and Digestibility*; American Society of Agronomy, Inc.: Madison, WI, USA, 1993; pp. 133–166. [CrossRef]
9. Mosier, N.; Wyman, C.; Dale, B.; Elander, R.; Lee, Y.Y.; Holtzapple, M.; Ladisch, M. Features of promising technologies for pretreatment of lignocellulosic biomass. *Bioresour. Technol.* **2005**, *96*, 673–686. [CrossRef] [PubMed]
10. McCann, M.C.; Carpita, N.C. Biomass recalcitrance: A multi-scale, multi-factor, and conversion-specific property. *J. Exp. Bot.* **2015**, *66*, 4109–4118. [CrossRef]
11. Barrière, Y.; Méchin, V.; Riboulet, C.; Guillaumie, S.; Thomas, J.; Bosio, M.; Fabre, F.; Goffner, D.; Pichon, M.; Lapierre, C.; et al. Genetic and genomic approaches for improving biofuel production from maize. *Euphytica* **2009**, *170*, 183–202. [CrossRef]
12. Selig, M.J.; Viamajala, S.; Decker, S.R.; Tucker, M.P.; Himmel, M.E.; Vinzant, T.B. Deposition of lignin droplets produced during dilute acid pretreatment of maize stems retards enzymatic hydrolysis of cellulose. *Biotechnol. Prog.* **2007**, *23*, 1333–1339. [CrossRef]
13. Mansfield, S.D.; Mooney, C.; Saddler, J.N. Substrate and enzyme characteristics that limit cellulose hydrolysis. *Biotechnol. Prog.* **1999**, *15*, 804–816. [CrossRef]

14. Berlin, A.; Balakshin, M.; Gilkes, N.; Kadla, J.; Maximenko, V.; Kubo, S.; Saddler, J. Inhibition of cellulase, xylanase and β-glucosidase activities by softwood lignin preparations. *J. Biotechnol.* **2006**, *125*, 198–209. [CrossRef] [PubMed]
15. Nakagame, S.; Chandra, R.P.; Saddler, J.N. The effect of isolated lignins, obtained from a range of pretreated lignocellulosic substrates, on enzymatic hydrolysis. *Biotechnol. Bioeng.* **2010**, *105*, 871–879. [CrossRef] [PubMed]
16. Torres, A.F.; Visser, R.G.F.; Trindade, L.M. Bioethanol from maize cell walls: Genes, molecular tools, and breeding prospects. *GCB Bioenergy* **2015**, *7*, 591–607. [CrossRef]
17. Ragauskas, A.J.; Beckham, G.T.; Biddy, M.J.; Chandra, R.; Chen, F.; Davis, M.F.; Davison, B.H.; Dixon, R.A.; Gilna, P.; Keller, M.; et al. Lignin valorization: Improving lignin processing in the biorefinery. *Science* **2014**, *344*, 6185. [CrossRef]
18. López-Malvar, A.; Butron, A.; Malvar, R.A.; McQueen-Mason, S.J.; Faas, L.; Gómez, L.D.; Revilla, P.; Figueroa-Garrido, D.J.; Santiago, R. Association mapping for maize stover yield and saccharification efficiency using a multiparent advanced generation intercross (MAGIC) population. *Sci. Rep.* **2021**, *11*, 1–9. [CrossRef]
19. Oliveira, D.M.; Mota, T.R.; Grandis, A.; Morais, G.R.D.; Lucas, R.C.D.; Polizeli, M.L.T.M.; Marchiosi, R.; Buckeridge, M.S.; Ferrarese-Filho, O.; Santos, W.D.D. Lignin plays a key role in determining biomass recalcitrance in forage grasses. *Renew. Energy* **2020**, *147*, 2206–2217. [CrossRef]
20. Costa, R.M.F.D.; Barrett, W.; Carli, J.; Allison, G.G. Analysis of Plant Cell Walls by Attenuated Total Reflectance Fourier Transform Infrared Spectroscopy. In *The Plant Cell Wall*; Humana: New York, NY, USA, 2020; pp. 97–313. ISBN 9781071606193.
21. Jiménez-Galindo, J.C.; Malvar, R.A.; Butrón, A.; Santiago, R.; Samayoa, L.F.; Caicedo, M.; Ordás, B. Mapping of resistance to corn borers in a MAGIC population of maize. *BMC Plant Biol.* **2019**, *19*, 1–17. [CrossRef]
22. Butrón, A.; Santiago, R.; Cao, A.; Samayoa, L.; Malvar, R. QTLs for Resistance to Fusarium Ear Rot in a Multiparent Advanced Generation Intercross (MAGIC) Maize Population. *Plant Dis.* **2019**, *103*, 897–904. [CrossRef]
23. Gomez, L.D.; Whitehead, C.; Barakate, A.; Halpin, C.; McQueen-Mason, S.J. Automated saccharification assay for determination of digestibility in plant materials. *Biotechnol. Biofuels* **2010**, *3*, 23. [CrossRef]
24. Faix, O. Classification of lignins from different botanical origins by FT-IR spectroscopy. *Holzforsch. Int. J. Biol. Chem. Phys. Technol. Wood* **1991**, *43*, 195–203. [CrossRef]
25. Kacuráková, M.; Capek, P.; Sasinková, V.; Wellner, N.; Ebringerová, A. FT-IR study of plant cell wall model compounds: Pectic polysaccharides and hemicelluloses. *Carbohydr. Polym.* **2000**, *43*, 195–203. [CrossRef]
26. Sills, D.L.; Gossett, J.M. Using FTIR to predict saccharification from enzymatic hydrolysis of alkali-pretreated biomasses. *Biotechnol. Bioeng.* **2012**, *109*, 353–362. [CrossRef] [PubMed]
27. Zhao, J.; Xiuwen, W.; Hu, J.; Liu, Q.; Shen, D.; Xiao, R. Thermal degradation of softwood lignin and hardwood lignin by TG-FTIR and Py-GC/MS. *Polym. Degrad. Stab.* **2014**, *108*, 133–138. [CrossRef]
28. Traoré, M.; Kaal, J.; Cortizas, A.M. Application of FTIR spectroscopy to the characterization of archeological wood. *Spectrochim. Acta Part A Mol. Biomol. Spectrosc.* **2016**, *153*, 63–70. [CrossRef] [PubMed]
29. Cuello, C.; Marchand, P.; Laurans, F.; Grand-Perret, C.; Lainé-Prade, V.; Pilate, G.; Déjardin, A. ATR-FTIR microspectroscopy brings a novel insight into the study of cell wall chemistry at the cellular level. *Front. Plant Sci.* **2020**, *11*, 1–13. [CrossRef]
30. Carpita, N.C.; Defernez, M.; Findlay, K.; Wells, B.; Shoue, D.A.; Catchpole, G.; Wilson, R.H.; McCann, M.C. Cell wall architecture of the elongating maize coleoptile. *Plant Physiol.* **2001**, *127*, 551–565. [CrossRef]
31. Kubo, S.; Kadla, J.F. Hydrogen bonding in lignin: A fourier transform infrared model compound study. *Biomacromolecules* **2005**, *6*, 2815–2821. [CrossRef]
32. McCann, M.C.; Defernez, M.; Urbanowicz, B.R.; Tewari, J.C.; Langewisch, T.; Olek, A.; Wells, B.; Wilson, R.H.; Carpita, N.C. Neural network analyses of infrared spectra for classifying cell wall architectures. *Plant Physiol.* **2007**, *143*, 1314–1326. [CrossRef]
33. Szymanska-Chargot, M.; Zdunek, A. Use of FT-IR Spectra and PCA to the bulk characterization of cell wall residues of fruits and vegetables along a fraction process. *Food Biophys.* **2013**, *8*, 29–42. [CrossRef]
34. Abidi, N.; Cabrales, L.; Haigler, C.H. Changes in the cell wall and cellulose content of developing cotton fibers investigated by FTIR spectroscopy. *Carbohydr. Polym.* **2014**, *100*, 9–16. [CrossRef] [PubMed]
35. Bekiaris, G.; Lindedam, J.; Peltre, C.; Decker, S.R.; Turner, G.B.; Magid, J.; Bruun, S. Rapid estimation of sugar release from winter wheat straw during bioethanol production using FTIR-photoacoustic spectroscopy. *Biotechnol. Biofuels* **2015**, *8*, 1–12. [CrossRef] [PubMed]
36. Lupoi, J.S.; Singh, S.; Parthasarathi, R.; Simmons, B.A.; Henry, R.J. Recent innovations in analytical methods for the qualitative and quantitative assessment of lignin. *Renew. Sustain. Energy Rev.* **2015**, *49*, 871–906. [CrossRef]
37. Christophe, F.; Séné, B.; Mccann, M.C.; Wilson, R.H.; Crinter, R. Fourier-transform Raman and Fourier-transform Lnfrared spectroscopy. *Plant Physiol.* **1994**, *106*, 1623–1631.
38. Pandey, K.K. A study of chemical structure of soft and hardwood and wood polymers by FTIR spectroscopy. *J. Appl. Polym. Sci.* **1999**, *71*, 1969–1975. [CrossRef]
39. Åkerholm, M.; Salmén, L. Interactions between wood polymers studied by dynamic FT-IR spectroscopy. *Polymer* **2001**, *42*, 963–969. [CrossRef]
40. McCann, M.C.; Bush, M.; Milioni, D.; Sado, P.; Stacey, N.J.; Catchpole, G.; Defernez, M.; Carpita, N.C.; Hofte, H.; Ulvskov, P.; et al. Approaches to understanding the functional architecture of the plant cell wall. *Phytochemistry* **2001**, *57*, 811–821. [CrossRef]
41. Schulz, H.; Baranska, M. Identification and quantification of valuable plant substances by IR and Raman spectroscopy. *Vib. Spectrosc.* **2007**, *43*, 13–25. [CrossRef]

42. Zhang, M.; Lapierre, C.; Nouxman, N.L.; Nieuwoudt, M.K.; Smith, B.G.; Chavan, R.R.; McArdle, B.H.; Harris, P.J. Location and characterization of lignin in tracheid cell walls of radiata pine (*Pinus radiata* D. Don) compression woods. *Plant Physiol. Biochem.* **2017**, *118*, 187–198. [CrossRef]
43. Marchessault, R.H. To cellulose and wood polysaccharides. *Pure Appl. Chem.* **1962**, *5*, 107–130. [CrossRef]
44. Harrington, K.J.; Higgins, H.G.; Michell, A.J. Infrared spectra of *Eucalyptus regnans* F. Muell. and *Pinus radiata* D. Don. *Holzforschung Int. J. Biol. Chem. Phys. Technol. Wood* **1964**, *18*, 108–113.
45. Blackwell, J. Infrared and Raman Spectroscopy of Cellulose. In *Cellulose Chemistry and Techology*; ACS: Washington, DC, USA, 1977; pp. 206–218.
46. Schwanninger, M.; Rodrigues, J.C.; Pereira, H.; Hinterstoisser, B. Effects of short-time vibratory ball milling on the shape of FT-IR spectra of wood and cellulose. *Vib. Spectrosc.* **2004**, *36*, 23–40. [CrossRef]
47. Vanholme, R.; Demedts, B.; Morreel, K.; Ralph, J.; Boerjan, W. Lignin biosynthesis and structure. *Plant Physiol.* **2010**, *153*, 895–905. [CrossRef] [PubMed]
48. Ding, S.Y.; Liu, Y.S.; Zeng, Y.; Himmel, M.E.; Baker, J.O.; Bayer, E.A. How does plant cell wall nanoscale architecture correlate with enzymatic digestibility? *Science* **2012**, *338*, 1055–1060. [CrossRef] [PubMed]
49. Weng, J.; Li, X.; Bonawitz, N.D.; Chapple, C. Emerging strategies of lignin engineering and degradation for cellulosic biofuel production. *Curr. Opin. Biotechnol.* **2008**, *19*, 166–172. [CrossRef] [PubMed]
50. Li, X.; Weng, J.K.; Chapple, C. Improvement of biomass through lignin modification. *Plant J.* **2008**, *54*, 569–581. [CrossRef]
51. Xiong, W.; Wu, Z.; Liu, Y.; Li, Y.; Su, K.; Bai, Z.; Guo, S.; Hu, Z.; Zhang, Z.; Bao, Y.; et al. Mutation of 4-coumarate: Coenzyme A ligase 1 gene affects lignin biosynthesis and increases the cell wall digestibility in maize brown midrib5 mutants. *Biotechnol. Biofuels* **2019**, *12*, 1–13. [CrossRef] [PubMed]
52. Huang, R.; Su, R.; Qi, W.; He, Z. Bioconversion of lignocellulose into bioethanol: Process intensification and mechanism research. *Bioenergy Res.* **2011**, *4*, 225–245. [CrossRef]
53. Fu, C.; Xiao, X.; Xi, Y.; Ge, Y.; Chen, F.; Bouton, J.; Dixon, R.A.; Wang, Z.Y. Downregulation of cinnamyl alcohol dehydrogenase (CAD) leads to improved saccharification efficiency in switchgrass. *Bioenergy Res.* **2011**, *4*, 153–164. [CrossRef]
54. Fornalé, S.; Capellades, M.; Encina, A.; Wang, K.; Irar, S.; Lapierre, C.; Ruel, K.; Joseleau, J.P.; Berenguer, J.; Puigdomènech, P.; et al. Altered lignin biosynthesis improves cellulosic bioethanol production in transgenic maize plants down-regulated for cinnamyl alcohol dehydrogenase. *Mol. Plant* **2012**, *5*, 817–830. [CrossRef]
55. Ralph, J.; Brunow, G.; Boerjan, W. Lignins. *Encycl. Life Sci.* **2007**, 1–10. [CrossRef]
56. Wilkerson, C.G.; Mansfield, S.D.; Lu, F.; Withers, S.; Park, J.Y.; Karlen, S.D.; Gonzales-Vigil, E.; Padmakshan, D.; Unda, F.; Rencoret, J.; et al. Monolignol ferulate transferase introduces chemically labile linkages into the lignin backbone. *Science* **2014**, *344*, 90–93. [CrossRef]
57. Costa, R.M.F.D.; Pattathil, S.; Avci, U.; Winters, A.; Hahn, M.G.; Bosch, M. Desirable plant cell wall traits for higher-quality miscanthus lignocellulosic biomass. *Biotechnol. Biofuels* **2019**, *12*, 1–18. [CrossRef]
58. Kumar, M.; Turner, S. Plant cellulose synthesis: CESA proteins crossing kingdoms. *Phytochemistry* **2015**, *112*, 91–99. [CrossRef]
59. Hall, M.; Bansal, P.; Lee, J.H.; Realff, M.J.; Bommarius, A.S. Cellulose crystallinity—A key predictor of the enzymatic hydrolysis rate. *FEBS J.* **2010**, *277*, 1571–1582. [CrossRef] [PubMed]
60. Nishiyama, Y.; Sugiyama, J.; Chanzy, H.; Langan, P. Crystal structure and hydrogen bonding system in cellulose Iα from synchrotron X-ray and neutron fiber diffraction. *J. Am. Chem. Soc.* **2003**, *125*, 14300–14306. [CrossRef]
61. Grantham, N.J.; Wurman-Rodrich, J.; Terrett, O.M.; Lyczakowski, J.J.; Stott, K.; Iuga, D.; Simmons, T.J.; Durand-Tardif, M.; Brown, S.P.; Dupree, R.; et al. An even pattern of xylan substitution is critical for interaction with cellulose in plant cell walls. *Nat. Plants* **2017**, *3*, 859–865. [CrossRef] [PubMed]
62. Busse-Wicher, M.; Gomes, T.C.F.; Tryfona, T.; Nikolovski, N.; Stott, K.; Grantham, N.J.; Bolam, D.N.; Skaf, M.S.; Dupree, P. The pattern of xylan acetylation suggests xylan may interact with cellulose microfibrils as a twofold helical screw in the secondary plant cell wall of *Arabidopsis thaliana*. *Plant J.* **2014**, *79*, 492–506. [CrossRef] [PubMed]
63. Pawar, P.M.A.; Derba-Maceluch, M.; Chong, S.L.; Gandla, M.L.; Bashar, S.S.; Sparrman, T.; Ahvenainen, P.; Hedenström, M.; Özparpucu, M.; Rüggeberg, M.; et al. In muro deacetylation of xylan affects lignin properties and improves saccharification of aspen wood. *Biotechnol. Biofuels* **2017**, *10*, 1–11. [CrossRef]